TECHNICAL NOTE

M. Alfano,[1] *F. Furgiuele,*[2] *L. Pagnotta,*[2] *and G. H. Paulino*[3]

Analysis of Fracture in Aluminum Joints Bonded with a Bi-Component Epoxy Adhesive

ABSTRACT: Adhesive bonding is a viable alternative to traditional joining systems (e.g., riveting or welding) for a wide class of components belonging to electronic, automotive, and aerospace industries. However, adhesive joints often contain flaws; therefore, the development of such technology requires reliable knowledge of the corresponding fracture properties. In the present paper, the candidate mode I fracture toughness of aluminum/epoxy joints is determined using a double cantilever beam fracture specimen. A proper data reduction scheme for fracture energy calculation has been selected based on the results of a sensitivity analysis. Furthermore, a scanning electron microscope is used in order to explore the locus of failure. Finally, the experimental findings are assessed by means of numerical simulations of crack growth carried out using a cohesive zone model.

KEYWORDS: epoxy adhesive, fracture, cohesive zone model

Introduction

Adhesive bonded joints have greatly attracted the interest of the designers from the automotive and aerospace industries because of the well-documented advantages they provide over the traditional joining technologies [1,2]. However, adhesive joints generally contain flaws and, during service, these flaws are likely to extend, thereby leading to nucleation of cohesive and/or interfacial macrocracks [2,3]. It follows that a safe joint design requires a reliable knowledge of the corresponding fracture resistance.

The commonly adopted test methods for assessing the performance of adhesive joints include the lap shear test, the pin-collar test, and the butt joint test [1,2]. These test methods assume a nominally uniform stress to exist on a defect free adhesive layer; therefore, they are not suitable for fracture resistance evaluation.

As a consequence, in the last decades, many efforts have been made in order to extend linear elastic fracture mechanics (LEFM) concepts to the analysis of fracture in adhesive joints. It has been shown that the fracture mechanics approach can lead to reliable and high performance joint design [4]. In particular, different kinds of fracture mechanics samples are currently available for fracture toughness estimation, e.g., the double cantilever beam (DCB) for mode I loading, the end notch flexure for mode II, and the Arcan sample for mixed mode loading; see Refs 5–8 to list a few.

The DCB is widespread for measuring mode I fracture energy

(G_{Ic}) of adhesive joints, and its use traces back to the 1960s [9,10]. In particular, the DCB is easily manufactured, and accurate data reduction schemes for the determination of G_{Ic} are available [10–14]. These calculation schemes have been improved through the years, thanks to the development of accurate models that estimate specimen compliance; for instance, the shear-corrected simple beam theory (SBT) was employed to take into account substrate shear deformations [10]. Accordingly, an ASTM standard was also proposed [11].

On the other hand, the SBT is not able to take into account beam root rotation arising from the presence of a flexible adhesive layer, i.e., the substrates do not act as built-in beams. To this aim, it was proposed to artificially increase the measured crack length using an experimentally derived correction term [12]. This modification was verified experimentally in [13] and incorporated in British standards [14]. The relations reported in Ref 14 have been employed to study, for instance, the effect of residual stresses on crack growth in DCB bonded samples [5,6], the fracture resistance of an epoxy resin in aqueous environment [7], and the crack growth behavior in a rubber-modified epoxy adhesive [15,16]. However, the accuracy on the determination of experimental variables, such as the crack length or specimen dimensions, obviously affects the results. Specifically, crack length measurement in samples bonded with toughened structural adhesives is somewhat difficult because crack growth often occurs in conjunction with damage development in the adhesive layer [15,16]. It follows that a data reduction scheme, which requires crack length as input in the calculation, could provide results affected by substantial errors. As a consequence, accurate estimations of fracture energy in adhesive bonded joint do require a careful choice of the data reduction scheme, and for this reason, a comparative analysis among those already available in the literature is needed.

The focus of this work is the analysis of mode I fracture toughness of aluminum/epoxy (AA6060-TA16/Hysol 9466) bonded joints. The Hysol 9466 (Loctite, Henkel, Germany) is a toughened, industrial grade epoxy suited for general purpose industrial applications. Recently, the bulk behavior of this epoxy adhesive was ex-

TABLE 1—*Material properties of the adhesive and the substrate.*

	AA6060-TA16	Loctite Hysol 9466
Young's modulus, E (GPa)	62.5[a]	1.7[b]
Poisson's ratio, ν	0.33[a]	0.35[c]
Tensile yielding strength, S_{yt} (MPa)	230[d]	30[e]
Compressive yielding strength, S_{yc} (MPa)	230[d]	55[e]
Glass transition temperature, T_g (°C)	N/A	62[f]

[a]Values obtained in the present work using the IET.
[b]Manufacturer' technical data sheets (ASTM D882).
[c]Typical value for epoxy adhesive.
[d]Values supplied by the manufacturer (www.migliarialluminio.it/).
[e]Reference 17.
[f]Manufacturer' technical data sheets (ASTM E1640-99).

amined carrying out tensile and compression tests [17]. In the present paper, the corresponding fracture toughness is assessed using DCB test coupons. In particular, a sensitivity analysis of G_{Ic} to the uncertainties on experimental variables is carried out to provide a rational basis for the choice of the most convenient calculation scheme. In addition, scanning electron microscopy (SEM) is executed for post-failure fracture surface examination. Finally, finite element (FE) simulations of crack growth, carried out using a cohesive zone model (CZM) [18–30], are employed in order to cross-check the obtained value of fracture energy. It is worth mentioning that although the mixed mode effect on joint fracture can be relevant, the focus of this work is limited to mode I fracture.

Materials and Methods

Specimen Preparation and Testing

The specimens analyzed consist of DCBs made of aluminum alloy (AA6060-TA16) substrates bonded with Hysol[®] 9466 (Henkel, Germany), a two component, medium viscosity, and fast curing toughened epoxy adhesive. The Hysol 9466 provides excellent bond strength to a wide variety of plastics and metals, and it is ideal for general purpose industrial applications requiring extended work life for adjusting parts during assembly. According to the manufacturers' data sheet, the Hysol 9466 develops high strength at room temperature after 24 h. Aluminum substrates were cut at a length $L=200\pm0.02$ mm from AA6060-TA16 extrusions of width $B=25\pm0.02$ mm and thickness $h=15\pm0.001$ mm.

Substrate and adhesive material properties are reported in Table 1.

As the stiffness of the substrate affects the accuracy of G_{IC}, the data provided by the manufacturer have been complemented by the authors using the impulse excitation technique (IET) [31]. In particular, the elastic modulus (E_s) has been estimated using the following expression:

$$E_s = 0.9465 \frac{m f_f^2}{B} \frac{L^3}{h^3} T_1 \qquad (1)$$

where:

m=mass of the test beam,
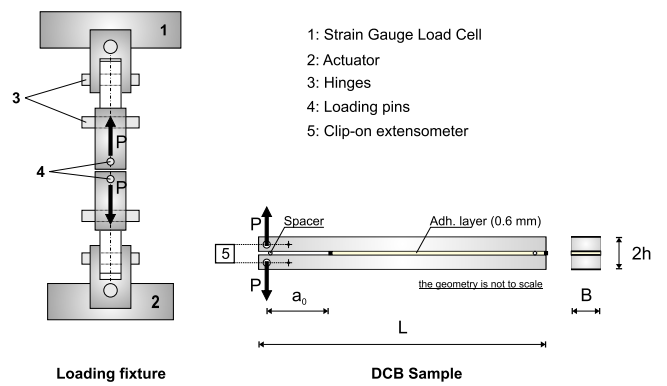f_f=fundamental natural frequency of vibration, and

FIG. 1—*Schematic of the fracture specimen (DCB) and the loading arrangement employed throughout the test.*

T_1=correction factor [31].

To this aim, beam-like specimens have been machined to the following nominal dimensions: $150\times25\times15$ mm³. The elastic modulus was found to be 65.7 GPa (scatter: 0.5 %). Substrate yield strength (S_y) provided by the manufacturer is equal to 230 MPa.

Specimen bonding and testing have been carried out according to the recommendation reported in Refs 11 and 14. Substrates surfaces were grit blasted (Alumina 80 grit) prior to bonding and then cleaned with tricloro-ethylene. The adhesive was then applied to substrate surfaces, and an un-bonded area was introduced using a release agent (liquid paraffin). An initial pre-crack (a_0) was subsequently created during testing by means of a loading-unloading cycle. An adhesive bond-line thickness nominally equal to h_a =0.6 mm (representative of practical applications) was ensured using metallic wires as spacers. Specimens were cured at room temperature (22°C) so that to tackle the occurrence of high residual stresses. A verification of the final bond-line thickness was carried out subtracting substrates thicknesses from the overall thickness of the specimen [14]. Three points along the length of the beam were selected to this purpose, at 30 mm from either ends, and at the mid length of the substrate. A layer thickness h_a =0.6±0.06 mm was recorded. In addition, this measurement was also verified using an optical microscope.

Tests were performed at room temperature using a universal testing machine (Instron 8500 plus). Specimens were pin-loaded and tested under displacement control at a constant cross-head feed rate of 0.06 mm/min [14]. The surfaces of the loading pins were lubricated to reduce frictional effects as much as possible. In addition, upper and lower loading frames were allowed to pivot about the centerline. In this manner, a cleavage opening was accommodated. In addition, in order to keep the specimen orthogonal to the load direction, the specimen-end opposite to the loading pins was supported before loading. A schematic illustration of the fracture specimen and of the loading fixture is reported in Fig. 1.

The crack mouth opening displacement (δ) was measured using a clip-on extensometer (Instron, 2630 series). The crack length was determined using a portable microscope; in order to facilitate the detection of crack growth, both sides of the bond line were coated with a thin layer of water-based typewriter correction fluid. Both specimen sides were monitored in order to assess any discrepancy in fracture propagation.

Data Reduction Schemes—Practical Aspects

According to the LEFM, the fracture energy for cracked plates can be estimated using the following expression [32]:

$$G_c = \frac{P_c^2}{2B}\left(\frac{dC}{da}\right)\Big|_{a=a_c} \qquad (2)$$

where:

$a =$ crack length,

$P_c =$ critical load, which corresponds to the critical crack length (a_c),

$B =$ width of the plate,

$C = \delta/P =$ compliance, and

$\delta =$ crack mouth opening displacement.

Therefore, Eq 2 allows one to determine the fracture energy of a test sample if the evolution of compliance with crack growth is known. In the case of DCB specimens, different data reduction schemes are available in the literature for fracture energy calculation [11,14]. Essentially, they differ on how dC/da is determined. For instance, the compliance method [14] requires a set of values for C to be determined as a function of a. The relation $C=C(a)$, obtained by fitting the experimental data points, is then differentiated and introduced in Eq 2. Therefore, given inputs as the critical load, the width, and dC/da, the fracture energy can be obtained. For instance, the method proposed in Ref 33 approximates the compliance by a power-law relation, $C(a)=ka^n$, from which one obtains[4]

$$G_{\mathrm{Ic}} = \frac{nP_c\bar{\delta}}{2Ba_c} \qquad (3)$$

where:

$\bar{\delta} =$ crack mouth opening at the critical load P_c.

On the other hand, the critical strain energy release rate can be derived from test results by means of specific models describing specimen compliance as a function of crack length. A number of theoretical expressions have been proposed stemming from the beam theory framework. For instance, the load-deflection equation of a built-in beam derived from the Euler–Bernoulli theory allows the compliance to be expressed as [32]

$$C = \frac{\delta}{P} = \frac{2a^3}{3E_s I} \qquad (4)$$

where:

$I =$ moment of inertia of substrate cross-section.

Combining Eqs 2 and 4, the mode I critical energy release rate can thus be expressed as

$$G_{\mathrm{Ic}} = \frac{12P_c^2 a_c^2}{B^2 E_s h^3} \qquad (5)$$

An alternative scheme can be obtained solving Eq 4 for load P, i.e.

$$P = \frac{3\,\delta E_s I}{2a^3} \qquad (6)$$

and substituting it in Eq 5 to obtain

$$G_{\mathrm{Ic}} = \frac{3P_c\bar{\delta}}{2Ba_c} \qquad (7)$$

This expression does not depend on h and is also used in British standards [14].

However, Eqs 5 and 7 are based on the Euler–Bernoulli beam theory, and therefore the effect of substrates shear deformation is

[4]k and n are determined by curve-fitting.

neglected. To circumvent this problem, other researchers proposed to include shear effect; in this case, specimen compliance becomes [10,34]

$$C = \frac{8a}{BE_s h^3}(a^2 + h^2) \qquad (8)$$

and therefore

$$G_{\mathrm{Ic}} = \frac{4P_c^2}{B^2 E_s}\left(\frac{3a_c^2}{h^3} + \frac{1}{h}\right) \qquad (9)$$

The second term in brackets represents the effect of substrate shear deformation; it is apparent that its contribution is negligible if $a \gg h$. ASTM D3433-05 [11] for cleavage testing of adhesive joints is based on Eq 9. This expression is also reported in a British standard [14]. However, it has been shown [12,35] that Eqs 5, 7, and 9 neglect the flexibility of the deforming adhesive layer and the (related) rotation of the adherents at the crack tip. In order to account for this root rotation, a correction factor a' can be used to artificially increase the crack length [36]. With such correction, Eq 9 can be rewritten as

$$G_{\mathrm{Ic}} = \frac{4P_c^2}{B^2 E_s}\left(\frac{3(a_c + a')^2}{h^3} + \frac{1}{h}\right) \qquad (10)$$

The correction factor needs to be determined experimentally. In particular, a least square linear plot of $C^{1/3}$ as a function of crack length should be generated so that its x-axis intercept yields a'. However, if $a > 2h$, then $a' \approx h/3$ [37]. This correction for beam root rotation can be also applied to Eq 7

$$G_{\mathrm{Ic}} = \frac{3P_c\bar{\delta}}{2B(a_c + a')} \qquad (11)$$

The previous expression is recommended in a British standard [14]. Finally, it is also possible to obtain an expression, which does not depend on crack length measurement, eliminating a from Eq 6 and substituting it in Eq 7, i.e.

$$G_{\mathrm{Ic}} = \frac{P_c^2}{BE_s I}\left[\frac{3E_s I\bar{\delta}}{2P_c}\right]^{2/3} \qquad (12)$$

It is worth noting that in Eq 12, the shear effect has been neglected; however, it has been shown [35] that it is a convenient analytical scheme for calculating fracture energy.

Sensitivity Analysis

It is important to assess how much a small uncertainty associated to the experimental measurements is amplified by the data reduction scheme selected for G_{Ic} calculation. A sensitivity analysis is suitable to the purpose because it allows the assessment of the robustness of model predictions. Fracture energy is a general function of the different experimental variables involved in the problem and can be expressed as a function of the following parameters:

$$G_{\mathrm{Ic}} = f(E_s, h, B, P_c, \bar{\delta}, a_c) \qquad (13)$$

A dimensionless number η_i is then defined as

$$\eta_i = \frac{x_i}{G_{\mathrm{Ic}}}\left|\frac{\partial G_{\mathrm{Ic}}}{\partial x_i}\right| \qquad (14)$$

where:

$x_i =$ generic experimental variable.

TABLE 2—*Absolute values of the sensitivity coefficients η_i associated with fracture energy calculation.*

Experimental Variable, x_i	Equation 9	Equation 11	Equation 12
Young's modulus, E_s	1.00	$\cdots$	0.33
Thickness, h	2.94	$\cdots$	1.00
Width, B	2.00	1.00	1.33
Load, P_c	2.00	1.00	1.33
Crack mouth opening, $\bar{\delta}$	$\cdots$	1.00	0.67
Crack length, a_c	1.94	1.00	$\cdots$

This quantity represents the sensitivity coefficient for uncertainty propagation [38]. Basically, it provides an indication of how the uncertainties associated to the experimental variables are amplified by the data reduction scheme chosen. Analytical expressions for η_i can be inferred using the explicit expression reported in the previous section. In particular, Eqs 9, 11, and 12 have been chosen for comparison purpose.

In Eq 11, there is an implicit assumption that no error is produced in the evaluation of the regression line that provides the correction factor a', which therefore is regarded as a constant. However, this is not the actual condition because the results provided by fitting procedures depend on the number of experimental points adopted in the calculations. The accuracy of the final results decreases if the method is applied when few experimental points are available. However, this uncertainty is neglected in our analysis. For this reason, Eq 7 would provide results similar to that obtained using Eq 11. In Table 2, the sensitivity coefficients for the different data reduction schemes are reported. It is apparent that Eq 9 is the most sensitive to measurement uncertainties on the experimental variables, and thus it will not be further considered in our discussion. On the other hand, Eqs 11 and 12 show lower sensitivity to the experimental variables.

In particular, they show similar sensitivity to the uncertainties affecting B, P_c, and $\bar{\delta}$ measurements, but these experimental variables can be usually determined with good reliability. However, Eq 11 does not depend on E_s and h, whereas Eq 12 does not depend on a_c. It is worth to point out that E_s and h measurements can be carried out, retaining the corresponding uncertainties to reasonable levels. As stated in the previous sections, E_s can be accurately determined using the IET, while h can be measured, for instance, using a digital micrometer that allows resolutions up to ± 0.001 mm. Instead, crack length measurement is difficult to be carried out because cracking in adhesive joints usually occurs with concurrent damage development and anticlastic bending curvature[5] of specimen arms. Furthermore, during testing, the specimen is observed from its edges only. It follows that the resulting uncertainty on a_c could be relatively large. Therefore, it would be advisable to eliminate experimental measurements of crack length from fracture energy determination.

Experimental Results

Several DCB fracture tests have been carried out. Each sample was pre-cracked prior to testing. An initial crack length equal to a_0 =(30±5) mm was observed. Sample load-crack mouth opening (P-δ) curves recorded during the test are reported in Fig. 2. Typically, the P-δ curve, after an initial linear response, deviates from linearity as a consequence of damage development in the deformed

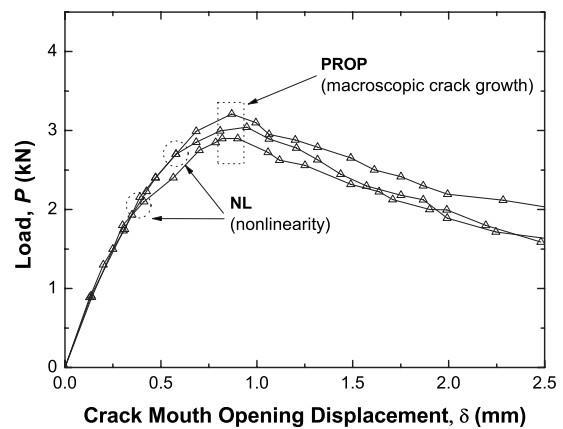[5]Secondary curvature in the direction perpendicular to the one of main bending.

FIG. 2—*Sample load versus crack mouth opening (P-δ) curve obtained during the tests (PROP: Macroscopic crack propagation; NL: Point at which deviation from linearity is observed).*

adhesive layer ahead of crack tip. Damage nucleation then occurs before the conditions for macroscopic crack growth onset are met. It has been observed during the tests that load deviates from linearity when it reaches the ~ 75 % of the peak load.

Afterward, when the maximum load is reached, the load-displacement curve starts to drop at a constant rate—the macroscopic crack propagation is assumed to begin at such a point. Subsequent crack growth was continuous without any occurrence of stick-slip behavior (slow stable extension). Therefore, no sharp drop in the P-δ curves was observed, and all the traces measured during the tests showed a similar behavior. The macroscopic deformation of the specimens was dominated by elasticity, and inelastic deformations were not observed after testing.

It is worth to point out that the estimation of crack length during the tests was difficult. Indeed, micro-cracking inside the adhesive layer did not allow easy identification of the crack tip position during crack extension.

Then, the fracture toughness of the joints was calculated using Eq 12, and the corresponding values were reported in Fig. 3 as a function of crack length (R-curve). The values of G_{Ic} first increase and then stabilize toward a constant value after further crack growth, i.e., when a macro-crack is fully developed.

Quantities of significance on the R-curve are the crack extension (Δa^*) necessary in order to attain the plateau and the corresponding fracture energy (G_{Ic}). During the experiments, $\Delta a^* \approx 10$ mm has been generally observed. A single-valued fracture toughness has
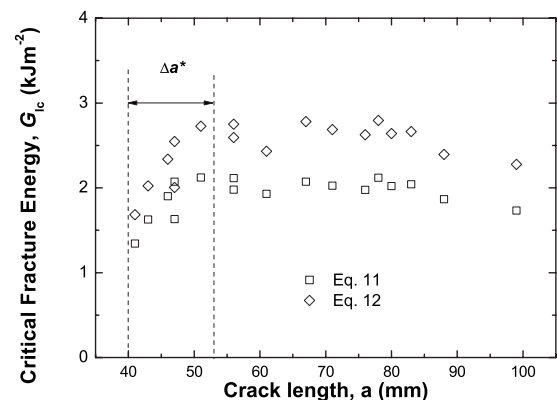

FIG. 3—*Typical set of crack growth resistance curves (R-curve).*

been calculated as an average of the values pertaining to the plateau region. It was found that $G_{\mathrm{Ic}} \approx 2.7$ kJ/m^2 (± 8 %). The total crack extension during experiments was found to be equal to $\Delta a = 60$ mm. The values obtained using Eq 11, reported in Fig. 3 for comparison, show that the fracture energy at first increases and then stabilizes toward a constant value in the plateau region. However, this value is somewhat different (≈ -26 %) from that calculated using Eq 12. The reason for this discrepancy could be attributed to the uncertainty on crack length measurement, which also affects the determination of the correction term (a'). This point will be further investigated in the next section.

A post-failure visual inspection of the fracture surfaces revealed that during the test, the crack kinked away from the lower to the upper (near) interfacial region and vice versa. Thus, an area of randomly shaped "island" of adhesive was generated on the substrates. In order to further assess the locus of failure, SEM analysis of fracture surfaces was carried out. To this aim, ad hoc samples were made cutting sections approximately 20×20 mm^2 from the failed specimens. The observed fracture surfaces are reported in Fig. 4.

Adhesive fracture was observed, as shown in Fig. 4(a) and 4(b), which illustrates typical fracture surfaces from the adherent and adhesive side, respectively. On the other hand, cohesive fracture was observed in the kink regions (Fig. 4(c)), when the crack runs from the upper to the lower interface. Crack kinking may lead to an increase of the fracture surfaces, and this, in turn, apparently results in the measured high value of fracture energy [1]. Therefore, the high bond toughness of the joint can be mainly attributed to this characteristic feature of crack path rather than to intrinsic properties of the adhesive itself.

Finite Element Simulations Using the Cohesive Zone Model

Theoretical Background and Modelling Approach

Numerical analyses of crack growth have been carried out using the CZM [18,19]. The basic aim of the numerical analyses reported herein is to cross-check the results reported in the previous section. According to CZM, the fracture process occurs in a lateral region (Fig. 5) in which a constitutive relation (the cohesive model) describes the evolution of cohesive tractions (T) as a function of crack surfaces displacements (Δ).

Various constitutive models have been proposed in order to investigate fracture in adhesive joints [28]. In all (intrinsic) models, the cohesive traction at first increases, reaches a maximum (σ_{cr}), and then gradually softens and falls to zero (ideally) when complete material separation occurs ($\Delta = \Delta_f$). The area under the T-Δ curve represents the cohesive fracture energy dissipated during crack growth (Γ). Provided that the conditions of LEFM hold, the cohesive fracture energy can be estimated from G_c [30].

The implementation of CZM in the FEM framework thus requires bulk FEs for modelling the background material and cohesive zone elements (CZEs) for modelling crack initiation, evolution, and complete failure. In summary, the cohesive element is formulated exploiting the principle of virtual work. The internal work done by the virtual strain (ε^*) in the domain (Ω) and the virtual crack opening displacement (Δ^*) along the crack line (Σ_c) is equal to the external work done by the virtual displacement ($\mathbf{u}^*$) at the traction boundary (Σ), i.e.
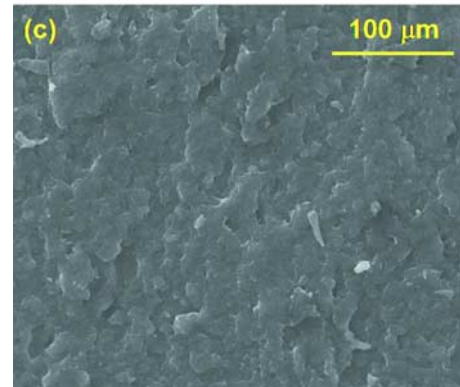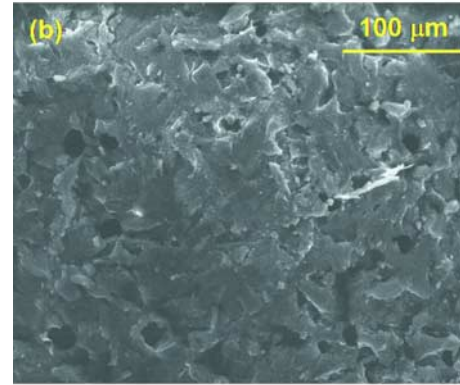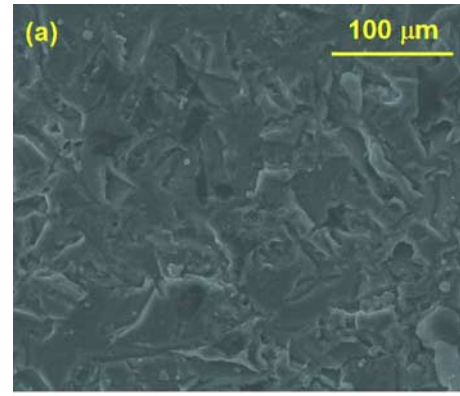

FIG. 4—*Post-failure SEM analyses showing the morphology of the fracture surfaces: (a) Adhesive side and (b) adherent side (crack growth from left to right); (c) cohesive fracture.*

$$\int_{\Omega} \boldsymbol{\sigma} : \boldsymbol{\varepsilon}^* d\Omega - \int_{\Sigma_c} \mathbf{T} \cdot \boldsymbol{\Delta}^* d\Sigma_c = \int_{\Sigma} \mathbf{P} \cdot \mathbf{u}^* d\Sigma \quad (15)$$

where:
$\mathbf{P}$ = external traction vector.

The crack face opening is interpolated to the Gauss integration points by means of standard shape functions, i.e.

$$\left[\int_{\Omega} \mathbf{B}^T \mathbf{E} \mathbf{B} d\Omega - \int_{\Sigma_c} \mathbf{N}_c^T \frac{\partial \mathbf{T}}{\partial \boldsymbol{\Delta}} \mathbf{N}_c d\Sigma_c \right] \mathbf{d} = \int_{\Sigma} \mathbf{N}^T \mathbf{P} d\Sigma \quad (16)$$

where:
$\mathbf{N}$ and $\mathbf{N}_c$ = matrices of the shape functions for bulk and cohesive elements, respectively,
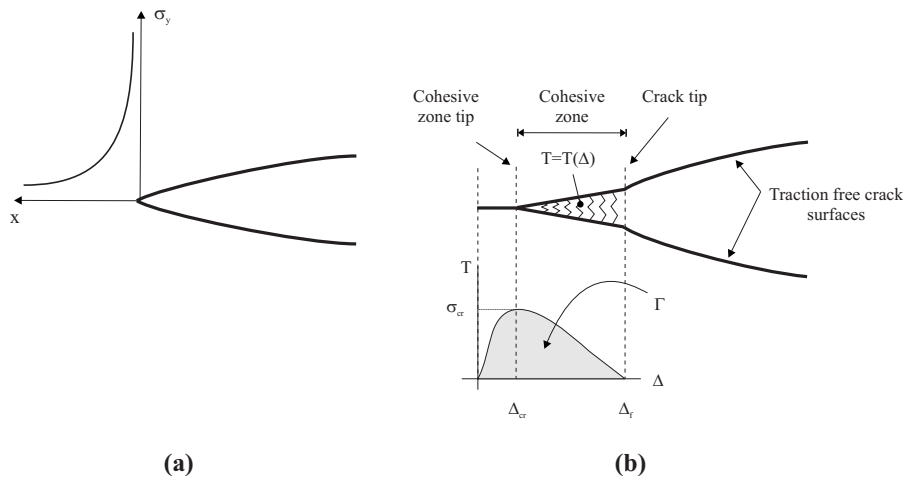$\mathbf{B}$ = derivative of $\mathbf{N}$,

(a) **(b)**

FIG. 5—*CZM concepts. (a) Singular region introduced by LEFM and (b) its replacement by cohesive fracture surfaces.*

d = nodal displacements, and

E = material tangential matrix for the bulk elements.

The stiffness matrix and load vector of the cohesive elements are assembled as a user-defined subroutine within the commercial FE code ABAQUS/Standard [39]. In particular, a detailed description of four-node CZEs formulation is reported elsewhere [28,40].

The specific shape of the cohesive model may play a role in the results; however, it has been demonstrated in Refs 28 and 40 that for this particular material system, the effect of the shape of the traction-separation relation is negligible. Therefore, the trapezoidal model [28] has been adopted in the simulations. In particular, this cohesive model is appropriate for modelling the undamaged state of cracked adhesive joints because it allows the control of the pre-peak slope of the traction-separation relation, thus reducing the artificial compliance introduced by the insertion of cohesive elements. However, because the crack path is pre-determined, such compliance is not a major issue [41].

The bond toughness for an adhesive layer usually involves two separate contributions, i.e., the intrinsic fracture energy (Γ_o) required for overcoming the intrinsic bonding forces and the visco-elastic and/or plastic energy term (Γ_p), which accounts for energy dissipation in the surrounding adhesive layer [1]. Therefore, a FE model accounting for the elasto-plastic behavior of the adhesive layer would be needed to demonstrate the effect of plastic dissipation on the bond toughness [25]. Nevertheless, in most cases, the adhesive layer is replaced by a single row of cohesive elements, and both the aforementioned energy contributing terms ($\Gamma = \Gamma_o + \Gamma_p$) are thus directly embodied in the traction-separation relation. Moreover, there is evidence that this simplified approach can provide accurate results [22–24,32]. It has been demonstrated that for thin adhesive layer (i.e., <1 mm) and moderately tough adhesives, the plastic dissipation is small compared to the intrinsic work of fracture, and a cohesive model that neglects the presence of the layer can be adopted to assess the integrity of adhesive joints [26,27]. Then, in the present work, the adhesive layer has been replaced by a single row of cohesive elements.

Further details regarding the FE model have been reported elsewhere [28,40]; therefore, we summarize herein the key features only. A four-node cohesive element was implemented in ABAQUS/Standard as a user-defined subroutine (user element). CZE size has been properly chosen to ensure that the results quoted in the paper were mesh independent (from a numerical viewpoint) and insensitive to numerical artefacts. To this aim, the total dissipated fracture energy has been computed for element sizes ranging from 0.01 to 1 mm. The dissipated energy was approximately constant for cohesive element size lower than 0.1 mm [40], and thus a cohesive element size equal to 0.08 mm was selected for the numerical simulations. In addition, plane strain continuum elements (ABAQUS CPE4) were adopted for sample substrates.

Numerical Results

Cohesive fracture parameters can be obtained by fitting model predictions to a set of experimental data [20–29]. It has been shown [25] that the rising portion of the P-δ curve of a DCB is sensitive to cohesive strength. After the peak load is reached (fully developed cohesive zone), the P-δ trace is essentially independent of cohesive strength, while the cohesive fracture energy starts playing a role. Indeed, provided that the global behavior of the specimen is linear elastic, the post-peak portion of the P-δ trace can be related to the opening displacement by the following equation [24]:

$$\left[\frac{(1-\nu^2)P}{E_s h_s}\right]^2 = \frac{1}{3\sqrt{3}}\left(\frac{(1-\nu^2)\Gamma}{E_s h_s}\right)^{3/2}\left(\frac{\delta}{h_s}\right)^{-1} \quad (17)$$
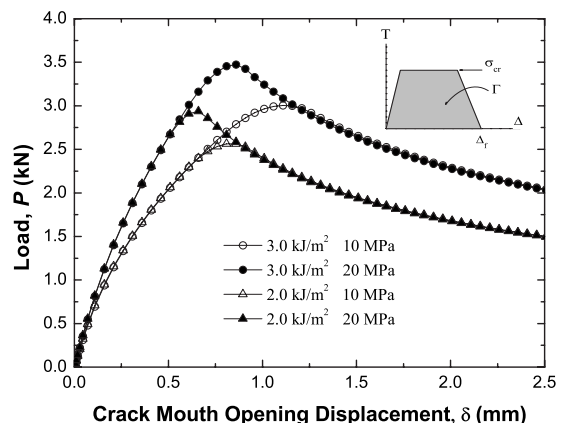
where all the symbols have been previously explained.

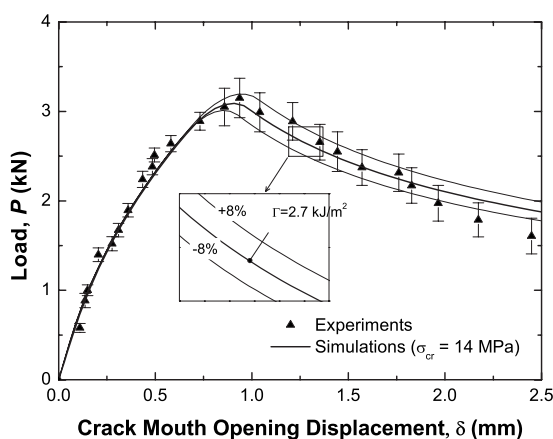FIG. 6—*Comparison of P-δ traces for different values of cohesive fracture energy and cohesive strength.*

FIG. 7—*Comparison between numerical and experimental P-δ curves.*

This dependence is also demonstrated in Fig. 6 where simulated P-δ curves corresponding to different values of fracture energy and cohesive strength are compared.

Notice that the post-peak region essentially depends on the input values of fracture energy whereas the peak load depends essentially on cohesive strength. It follows that the magnitude of cohesive fracture energy can be identified by matching experiments and simulations in the post-peak region of the P-δ trace. This feature represents a useful cross-check of the results calculated using Eq 12. In particular, the numerical P-δ curves, which provide the best fit with the data of the DCB test, are reported in Fig. 7.

In these simulations, a constant value of the cohesive strength has been set to 14 MPa as it allows to better capture the maximum experimental load. The fracture energy was then tuned in order to achieve a match between experiments and simulations. The value of cohesive fracture energy, which gave the best fit with the experiments, is in good agreement with the experimental value obtained using Eq 12. Therefore, the difference between the results provided by the data reduction scheme analyzed in the previous section may be attributed to the uncertainty on crack length measurement.

Conclusions

In this paper, the mode I fracture toughness of aluminum DCB joints bonded with a toughened epoxy adhesive was analyzed. The critical strain energy release rate as well as the crack growth resistance curve of the joint has been determined. To this aim, a suitable data reduction scheme, which does not depend on crack length measurement, was chosen based on the results of sensitivity analysis. The obtained fracture energy (2.7 ± 8 % kJ/m^2) was found to be ~26 % higher than that provided using the relations of a British standard. Therefore, the CZM was utilized in conjunction with the experimental findings to cross-check results consistency. Using the calculated fracture toughness as input in the simulations, agreement with the experiments could be achieved, thus supporting the consistency of the experimental procedures employed.

Finally, SEM analyses of fracture surfaces illustrated that fracture was essentially adhesive (adhesive/substrate interface). In particular, crack kinking from the lower to the upper interface provided an increase of the fracture surfaces, and this, in turn, apparently resulted in the high value of the calculated fracture energy. A follow-up work will consider mixed mode fracture behavior of the

joints as well as the proper surface treatment which could promote a fully in layer cohesive fracture.

References

[1] Kinloch, J., *Adhesion and Adhesives: Science and Technology*, Chapman & Hall, London, 1987.
[2] Messler, R. W., *Joining of Materials and Structures*, Elsevier, Oxford, 2004.
[3] ISO 10365:1992(E), 1992, "Adhesives—Designation of Main Failure Patterns," International Organization for Standardization, Geneve, Switzerland.
[4] Kinloch, A. J., "Adhesives in Engineering," *Proceedings of the Institution of Mechanical Engineers, Part G: Journal of Aerospace Engineering*, Vol. 211(5), 1997, pp. 307–335.
[5] Chen, B. and Dillard, D. A., "Numerical Analysis of Directionally Unstable Crack Propagation in Adhesively Bonded Joints," *Int. J. Solids Struct.*, Vol. 38(38–39), 2001, pp. 6907–6924.
[6] Chen, B. and Dillard, D. A., "The Effect of the T-Stress on Crack Path Selection in Adhesively Bonded Joints," *Int. J. Adhes. Adhes.*, Vol. 21(5), 2001, pp. 357–368.
[7] Kinloch, A. J., Korenberg, C. F., Tan, K. T., and Watts, J. F., "Crack Growth in Structural Adhesive Joints in Aqueous Environments," *J. Mater. Sci.*, Vol. 42(15), 2007, pp. 6353–6370.
[8] Choupani, N., "Mixed-Mode Cohesive Fracture of Adhesive Joints: Experimental and Numerical Studies," *Eng. Fract. Mech.*, Vol. 75(15), 2008, pp. 4363–4382.
[9] Mostovoy, S. and Ripling, E. J., "Effect of Joint Geometry on the Toughness of Epoxy Adhesives," *J. Appl. Polym. Sci.*, Vol. 15(3), 1971, pp. 661–673.
[10] Mostovoy, S., Crosley, P. B., and Ripling, E. J., "Use of Crack-Line-Loaded Specimens for Measuring Plane Strain Fracture Toughness," *J. Mater.*, Vol. 2, 1967, pp. 661–681.
[11] ASTM Standard D3433-05, 2005, "Standard Test Method for Fracture Strength in Cleavage of Adhesives in Bonded Metal Joints," *Annual Book of ASTM Standards*, Vol. 15.06, ASTM International, West Conshohocken, PA.
[12] Blackman, B., Dear, J. P., Kinloch, A. J., and Osiyemi, S., "The Calculation of Adhesive Fracture Energies from Double-Cantilever Beam Test Specimens," *J. Mater. Sci. Lett.*, Vol. 10, 1991, pp. 253–256.
[13] Blackman, B., Kinloch, A. J., Paraschi, M., and Teo, W. S., "Measuring the Mode I Adhesive Fracture Energy, G$_{IC}$, of structural Adhesive Joints: The Results of an International Round-Robin," *Int. J. Adhes. Adhes.*, Vol. 23(4), 2003, pp. 293–305.
[14] BS7991, 2001, "Determination of the Mode I Adhesive Fracture Energy, G$_{IC}$, of Structural Adhesives Using the Double

Cantilever Beam (DCB) and Tapered Double Cantilever Beam (TDCB) Specimens," British Standard Institution, London, United Kingdom.

[15] Imanaka, M., Orita, R., Nakamura, Y., and Kimoto, M., "Comparison of Failure Mechanisms Between Rubber-Modified and Unmodified Epoxy Adhesives Under Mode II Loading Condition," *J. Mater. Sci.*, Vol. 43(9), 2008, pp. 3223–3233.

[16] Imanaka, M., Motohashi, S., Nishi, K., Nakamura, Y., and Kimoto, M., "Crack-Growth Behaviour of Epoxy Adhesives Modified with Liquid Rubber and Cross-Linked Rubber Particles Under Mode I Loading," *Int. J. Adhes. Adhes.*, Vol. 29(1), 2009, pp. 45–55.

[17] Goglio, L., Peroni, L., Peroni, M., and Rossetto, M., "High Strain-Rate Compression and Tension Behaviour of an Epoxy Bi-Component Adhesive," *Int. J. Adhes. Adhes.*, Vol. 28(7), 2008, pp. 329–339.

[18] Dugdale, D. S., "Yielding Steel Sheets Containing Slits," *J. Mech. Phys. Solids*, Vol. 8, 1960, pp. 100–104.

[19] Barenblatt, G. I., "Mathematical Theory of Equilibrium Cracks in Brittle Fracture," *Adv. Appl. Mech.*, Vol. 7, 1962, pp. 55–129.

[20] Scheider, I. and Brocks, W., "Cohesive Elements for Thin Walled Structures," *Comput. Mater. Sci.*, Vol. 37(1–2), 2006, pp. 101–109.

[21] Song, S. H., Paulino, G. H., and Buttlar, W. G., "Simulation of Crack Propagation in Asphalt Concrete Using an Intrinsic Cohesive Zone Model," *J. Eng. Mech.*, Vol. 132(11), 2006, pp. 1215–1223.

[22] Sun, C., Thouless, M. D., Waas, A. M., Schroeder, J. A., and Zavattieri, P. D., "Ductile-Brittle Transitions in Adhesively Bonded Structures. Part I: Experimental Studies," *Int. J. Solids Struct.*, Vol. 45(10), 2008, pp. 3059–3073.

[23] Sun, C., Thouless, M. D., Waas, A. M., Schroeder, J. A., and Zavattieri, P. D., "Ductile-Brittle Transitions in Adhesively Bonded Structures. Part II: Numerical Studies," *Int. J. Solids Struct.*, Vol. 45(17), 2008, pp. 4725–4738.

[24] Li, S., Thouless, M. D., Waas, A. M., Schroeder, J. A., and Zavattieri, P. D., "Use of Mode-I Cohesive-Zone Models to Describe the Fracture of an Adhesively-Bonded Polymer-Matrix Composite," *Compos. Sci. Technol.*, Vol. 65(2), 2005, pp. 281–293.

[25] Yuan, H. and Xu, Y., "Computational Fracture Mechanics Assessment of Adhesive Joints," *Comput. Mater. Sci.*, Vol. 43(1), 2008, pp. 146–156.

[26] Pardoen, T., Ferracin, T., Landis, C. M., and Delannay, F., "Constraint Effect in Adhesive Joint Fracture," *J. Mech. Phys. Solids*, Vol. 53(9), 2005, pp. 1951–1983.

[27] Martiny, P., Lani, F., Kinloch, A. J., and Pardoen, T., "Numeri-cal Analysis of the Energy Contributions in Peel Tests: A Steady-State Multilevel Finite Element Approach," *Int. J. Adhes. Adhes.*, Vol. 28(4–5), 2008, pp. 222–236.

[28] Alfano, M., Furgiuele, F., Leonardi, A., Maletta, C., and Paulino, G. H., "Analysis of Mode I Fracture in Adhesive Joints Using Tailored Cohesive Zone Models," *Int. J. Fract.*, Vol. 157(1–2), 2009, pp. 193–204.

[29] Liljedahl, C. D. M., Crocombe, A. D., Wahab, M. A., and Ashcroft, I. A., "Damage Modelling of Adhesively Bonded Joints," *Int. J. Fract.*, Vol. 141(1–2), 2006, pp. 147–161.

[30] Allix, O. and Corigliano, A., "Modeling and Simulation of Crack Propagation in Mixed-Modes Interlaminar Fracture Specimens," *Int. J. Fract.*, Vol. 77(2), 1996, pp. 111–140.

[31] ASTM E1876-09, 2009, "Standard Test Method for Dynamic Young's Modulus, Shear Modulus, and Poisson's Ratio by Impulse Excitation of Vibration," *Annual Book of ASTM Standards*, Vol. 03.01, ASTM International, West Conshohocken, PA.

[32] Anderson, T. L., *Fracture Mechanics, Fundamentals and Applications*, CRC Press, Boca Raton, FL, 2004.

[33] Berry, J. P., "Determination of Fracture Surface Energies by the Cleavage Techniques," *J. Appl. Phys.*, Vol. 34(1), 1963, pp. 62–68.

[34] Ripling, E. J., Mostovoj, S., and Patrick, R. L., "Measuring Fracture Toughness of Adhesive Joints," *Mater. Res. Stand.*, Vol. 4(3), 1964, pp. 129–134.

[35] Tamuzs, V., Tarasovs, S., and Vilks, U., "Delamination Properties of Translaminar-Reinforced Composites," *Compos. Sci. Technol.*, Vol. 63(10), 2003, pp. 1423–1431.

[36] Hashemi, S., Kinloch, A. J., and Williams, J. G., "Mechanics and Mechanism of Delamination in Poly(Ether Sulphone)-Fibre Composite," *Compos. Sci. Technol.*, Vol. 37(4), 1990, pp. 429–462.

[37] Tada, H., Paris, P. C., and Irwin, G. R., *The Stress Analysis of Cracks Handbook*, ASME Press, New York, 2000.

[38] International Organization for Standardization, *Guide to the Expression of Uncertainty in Measurement*, International Organization for Standardization, Geneva, Switzerland, 1995, ISBN 92-67-10188-9.

[39] ABAQUS User's Manual; v6.5-1. (2002). Hibbit, HKS, Inc., Pawtucket, RI.

[40] Alfano, M., "Cohesive Zone Modeling of Mode I Fracture in Adhesive Joints," *Internal Communication*, University of Illinois at Urbana-Champaign, Urbana, IL, 2006 (available upon request).

[41] Zhang, Z. and Paulino, G. H., "Cohesive Zone Modeling of Dynamic Failure in Homogeneous and Functionally Graded Materials," *Int. J. Plast.*, Vol. 21(6), 2005, pp. 1195–1254.